Improving Machinability of High Chromium Wear Resistant Materials via Laser–assisted Machining

Journal:	*Machining Science and Technology*
Manuscript ID:	LMST-2012-0041.R1
Manuscript Type:	original scientific papers
Date Submitted by the Author:	14-Jun-2012
Complete List of Authors:	Ding, Hongtao; Purdue University, Mechanical Engineering Shin, Yung; Purdue University, Mechanical Engineering
Keywords:	Laser-assisted machining, High chromium wear resistant materials, Tool wear, Surface integrity

Improving Machinability of High Chromium Wear Resistant Materials via Laser–assisted Machining

Hongtao Ding and Yung C. Shin*[1]

Center for Laser-based Manufacturing, School of Mechanical Engineering, Purdue University, West Lafayette, IN 47907, USA

Abstract

The machinability of high chromium wear resistant materials is poor due to their high hardness with a large amount of hard chromium carbides. This study is focused on improving the machinability of high chromium wear resistant materials with different microstructures and hardness levels via laser-assisted machining (LAM). A laser pre-scan process is designed to preheat the workpiece before LAM to overcome the laser power constraint. A transient, three-dimensional LAM thermal model is expanded to include the laser pre-scan process, and is validated through experiments using an infrared camera. The machinability of highly alloyed wear resistant materials of 27% and 35% chromium content is evaluated in terms of tool wear, cutting forces, and surface integrity through LAM experiments using CBN tools. With increasing material removal temperature from room temperature to 400°C, the benefit of LAM is demonstrated by 28% decrease in specific cutting energy, 50% improvement in surface roughness and a 100% increase in CBN tool life over conventional machining.

Keywords: Laser-assisted machining; High chromium wear resistant materials; Tool wear; Surface integrity

[1] Corresponding author: shin@purdue.edu, 01-765-494-9775, 585 Purdue Mall, Purdue University, West Lafayette, IN 47907, U.S.A.

INTRODUCTION

High chromium cast irons are white cast irons alloyed with 12 to 35% chromium and generally fall into a category defined by ASTM A 532 standard (Lampman and Zorc, 1990). These materials are commonly used for materials handling in the mining and minerals processing industries because of their exceptional wear resistance, which is a result of the large volume fraction of primary and/or eutectic chromium carbides in their microstructures (Lampman and Zorc, 1990; Tabrett et al., 1996). For instance, they have been used in slurry pumps where the sand and metallic particles effectively act as miniature cutting tools on the inner surfaces of pumps. The demand for mining equipment with a longer life span has led to the development of harder and more wear resistant materials with higher chromium content. High chromium content forms a large amount of chromium carbides and results in a hardness of 60 Rockwell C scale (HRC) and higher (Lampman and Zorc, 1990).

Use of conventional machining processes is difficult and expensive for high chromium white cast irons because of attendant slow machining speeds and/or frequent tool changes due to short tool life. The wear resistant materials can rapidly deteriorate the ceramic and tungsten carbides cutting tools due to the high amount of the extremely hard chromium carbides constituents (Zhou and Andersson, 2008). Currently, the state of the art technology for machining these materials generally relies on cubic boron nitride (CBN) and polycrystalline CBN (PCBN) tools, which are expensive and can be one of the highest contributors to the final cost of a machined part (Zhou and Andersson, 2008; Masood et al., 2011; Shen et al., 2010). CBN tools have increased the rate of productivity for difficult to machine alloys, but their use is still constrained by rapid tool wear or chipping, resulting in short tool lives. Shen et al. (2010) applied PCBN tools for turning of white cast iron with 26% chromium content and found that compared with ceramic tools PCBN tools can work at a relatively higher cutting speed and material removal rate. The preferable cutting speeds were determined to be 65-90 m/min and 80-120

m/min for rough and finish turning operations, respectively. Ren et al. (2001) conducted the machining tests of high chromium alloyed materials with the hardness of 55-58 HRC using PCBN tools and found that the main tool wear modes were edge chipping and flank wear at cutting speeds of 32-85 m/min. Zhou and Andersson (2008) experimentally evaluated the machinability of high chromium cast irons with PCBN cutting tools and found that the optimal cutting speed was 70 m/min to achieve the longest tool life and a maximum volume of material removal. In these studies, tool flank wear is found to be a decisive factor to limiting tool life in turning high chromium white cast irons, and the surface finish tends to deteriorate rapidly as tool wear becomes large.

In order to reduce the cost and improve the machinability of these materials, laser-assisted machining (LAM) is investigated in this study. During LAM, the workpiece material is locally heated and softened by a focused laser beam and then removed by a conventional cutting tool. By elevating the temperature and lowering the material strength in the cutting zone, LAM can achieve lower cutting forces, slower tool wear progression, higher material removal rate and better surface quality (Anderson et al., 2006; Ding and Shin, 2012; Suthar et al., 2008). When white cast irons with 24-33% chromium content are heated to a temperature within 400-600 °C, the mechanical strength and hardness decrease to a half of their values at room temperature (Lampman and Zorc, 1990; Davis, 1996; Belyakova et al., 1975). Masood et al. (2011) conducted a LAM study of white cast iron with 27% chromium content and found that compared with conventional cutting, the average cutting and feed forces in LAM were reduced by 8.3% and 12% at a cutting speed of 50 m/min using a CBN tool. The 10% force reduction in their study was not significant enough to achieve beneficial effects in tool performance and material removal. The study also did not provide an analysis of tool wear and surface integrity produced by LAM.

Precise control of the workpiece temperature is essential to implementing the LAM process. LAM studies have shown that operation parameters such as laser power, laser lead distance to the tool, cutting speed, feed, etc. can greatly affect the material temperature in the cutting zone and the resulting cutting forces (Ding and Shin, 2010; Sun et al., 2010; Germain et al., 2011). Three-dimensional (3D) transient thermal models have been developed to facilitate the design and analysis of LAM processes by the authors' group (Rozzi et al., 2000; Tian and Shin, 2006). The thermal model allows for precise control of the average material removal temperature (T_{mr}) in the cutting area during LAM of various work materials and cutting conditions, e.g., 400 °C for cutting of Waspaloy at cutting speed of 60-180 m/min (Ding and Shin, 2012). With the use of the thermal model, LAM has shown its advantages over conventional machining methods in terms of surface finish, tool wear, specific cutting energy, and subsurface integrity for various difficult-to-machine metal alloys, such as nickel-based superalloys (Anderson et al., 2006; Ding and Shin, 2012), titanium alloy TI6Al4V (Dandekar et al., 2010), hardened steels (Ding and Shin, 2010), and compacted graphite iron (CGI) (Skvarenina and Shin, 2006).

The objective of the present study is to improve the machinability of high chromium wear resistant materials with different microstructures and hardness levels via LAM. The study predicts the temperature fields within high chromium white cast iron workpieces undergoing laser heating, and investigates the effects of temperature and cutting conditions on tool wear, material removal rate, and surface integrity.

WORK MATERIALS

Three high chromium wear resistant materials were investigated in this study with different chromium contents of 27% (alloy 27%Cr), 30% (alloy 30%Cr) and 35% (alloy 35%Cr). These alloys

can be effectively used in a wide range of slurry types offering varying performances in erosion/corrosion resistance. Their excellent wear resistance is provided mainly by the presence of hard carbides in the microstructure. The microstructures of high-Cr cast irons consist of hard eutectic carbides (M_7C_3) and primary carbide (M_3C) in a ferrous matrix of martensite with some retained austenite. The differences among the three materials are in their chromium content, the amount of chromium carbides and hardness. Table 1 shows the phase compositions and physical properties of the three high-Cr cast irons. 27%Cr primarily consists of an eutectic phase composition, while 30%Cr and 35%Cr consist of both eutectic and primary carbides. Hardness and wear resistance of these materials are improved by increasing the amount of chromium carbide, which is a very hard phase but also very brittle. The average bulk hardness at room temperature was measured to be about 60 and 66 HRC for the as-received 27%Cr and 35%Cr parts, respectively. When temperature is elevated to above 400 °C, the hardness of all the three high-Cr white irons drastically drops. A main task of this study was to determine an optimal temperature at which LAM shows the most benefits.

The material thermal properties at elevated temperatures are critical to the accuracy of the temperature prediction by the LAM thermal model. The thermal conductivity and specific heat properties of the three materials are shown in Fig. 1 from room temperature up to 1200 °C, which were provided by Thermophysical Properties Research Laboratory (TPRL). It can be seen that the thermal conductivity decreases as the chromium carbide content increases, while it increases with temperature. The peaks in the specific heat are caused by the phase change around 750 °C (Belyakova et al., 1975).

EXPERIMENTAL SETUP

Laser-assisted turning experiments were performed with the high chromium white iron workpieces on a 20 horsepower Jones and Lambson CNC lathe equipped with a NUM 1060 controller.

The spindle motor is capable of providing a maximum of 2,600 rpm. Translating together with the cutting tool, a 10.6 micron wavelength CO_2 laser (Convergent Energy Everlase S51) irradiates the workpiece continuously ahead of the tool. During the experiments of LAM, the laser-tool lead angle was fixed at 55° for parts with different diameters. Fig. 2 (a) shows the schematic of the experimental setup, and (b) shows the laser beam in the machined chamfer. The cutting tools used were 3/8 inch square inserts of high CBN-content (Kennametal, grade KD200) with -5° rake angle, 15° lead angle and 0.8 mm nose radius (r_n). Prior to each machining experiment, the workpiece surface was sandblasted, cleaned, measured, and painted with a graphite adhesive powder/binder mixture (Cotronics 931) to increase the absorption of the metal at the CO_2 laser wavelength.

The maximum achievable CO_2 laser power is about 1200 W. With this maximum laser power, the achievable T_{mr} is less than 300 °C for a 50 mm diameter part under a cutting speed of 90 m/min and a feed of 0.075 mm/rev. Since a temperature of 300 °C does not soften the workpiece material enough, a laser preheating process was designed prior to the LAM process. This process increases the initial bulk temperature of the workpiece and overcomes the limitation of laser power for heating large high chromium alloy parts. During the preheating step, the laser scans across the surface of the parts without any material removal. This is followed by a normal LAM process, during which the laser heats the workpiece prior to the tool position, while the tool removes the material.

The two-step process of laser pre-scan and LAM with a moderate laser power satisfies the temperature increase requirement. The resulting smaller temperature gradient introduced by the two-step process helps alleviate the probability of crack generation on the workpiece surface for both 27%Cr and 35%Cr, which have a poor thermal shock resistance (Lampman and Zorc, 1990). Since the laser pre-scan step should not introduce any hardening effect to the workpiece, surface hardness was measured in and out of laser scanned areas to determine if there was any laser hardening effect. The

hardness measurements show that the average hardness was 59.1 HRC inside the laser scanned area, which was slightly less than the hardness of 60.1 HRC of the initial bulk material.

Force data were collected during machining using a three component Kistler 9121 dynamometer and a Kistler Model 5184B1 amplifier. A LabView program was used to record and process the signals for cutting force and laser power. Temperature measurements were performed using a FLIR SC3000 infrared camera with the ThermoCAM2002 software. The tool wear was examined with a Zeiss optical microscope. The surface roughness was measured using a Surtronic 3+ surface profilometer with a 5µm diamond stylus and also examined by an interferometric surface profiler MicroXAM. Arithmetic average values R_a were measured nine times along the feed direction from each machined workpiece and averaged to provide the surface roughness data. During LAM, the laser heating has the possibility of slightly oxidizing the machined surface in air. Therefore, the machined surface after the experiment was carefully checked for any discoloration. The workpiece material thermal expansion, caused by laser heating, causes a larger depth of cut during LAM than the designed value. However, Ding and Shin (2010) have demonstrated in their LAM experiments of hardened steel parts that a tight tolerance of final part diameter can be achieved. The final part dimension was machined by employing the cutting tool at the same radial position, despite the variations of the original part diameters and thermal expansion. In this study, to check for the consistency of the part dimension, the actual depth of cut was measured nine times at different locations of the machined workpiece at room temperature.

An abrasive cutoff wheel was used for initial sectioning of the large workpiece with the adequate and uniformly distributed coolant flow to minimize heat-induced damage. The specimens were prepared by following the standard metallographic preparation techniques, i.e., sectioning with an abrasive cutoff wheel, grinding and polishing with diamond paste and then were chemically etched in Glycergia solution (3 parts glycerine, 2 parts hydrochloric acid (HCl), 1 part nitric acid (HNO3)).

Metallographic samples were examined using an optical microscope. Surface hardness and subsurface microhardness were measured using a Mitutoyo ATK-F1000 hardness tester and a Vickers hardness tester, respectively.

THERMAL MODELING

It is necessary to precisely determine the temperature field in a rotating workpiece undergoing laser heating to maximize the benefits of thermal softening effects while ensuring proper heating of the workpiece.

Thermal modeling

A transient, three-dimensional thermal model was first developed by Rozzi et al. (2000) for an opaque rotating workpiece during LAM. Later, Tian and Shin (2006) enhanced the capabilities of the thermal model by changing it from a stationary laser/moving workpiece (Eulerian approach) to a fixed workpiece/moving laser (Lagrangian approach) and also by including adaptive geometry change to simulate LAM of complex geometry. Eq. 1 shows the governing heat transfer equation:

$$\rho\left(\frac{\partial h}{\partial t}+\omega\frac{\partial h}{\partial \varphi}\right)=\frac{1}{r}\frac{\partial}{\partial r}\left(rk\frac{\partial T}{\partial r}\right)+\frac{1}{r^2}\frac{\partial}{\partial \varphi}\left(k\frac{\partial T}{\partial \varphi}\right)+\frac{\partial}{\partial z}\left(k\frac{\partial T}{\partial z}\right)+S \qquad (1)$$

where ρ is density, ω is the angular velocity, h is enthalpy, and T is temperature, while r, φ and z are cylindrical coordinates. The first term on the left-hand side of Eq. 1 represents energy storage, and the other comes from circumferential advection due to the rotation of workpiece relative to the coordinate system. The first three terms on the right-hand side of Eq. 1 represent energy diffusion in the radial, circumferential and axial directions, respectively. The last expression is a source term for internal heat generation. In the finite volume scheme developed by Tian and Shin (2006), Eq. 1 was rewritten in the form of Eq. 2 to facilitate the numerical solution of the heat transfer problem in LAM, where the

material may experience temperatures higher than 1000 °C and the temperature dependence of material thermophysical properties has to be taken into account:

$$\rho\left(\frac{\partial\left(c_p T\right)}{\partial t}+\omega\frac{\partial\left(c_p T\right)}{\partial \varphi}\right)=\frac{1}{r}\frac{\partial}{\partial r}\left(rk\frac{\partial T}{\partial r}\right)+\frac{1}{r^2}\frac{\partial}{\partial \varphi}\left(k\frac{\partial T}{\partial \varphi}\right)+\frac{\partial}{\partial z}\left(k\frac{\partial T}{\partial z}\right)+S+\rho\frac{\partial}{\partial t}\left(c_p T^{*}-h^{*}\right)+\rho\omega\frac{\partial}{\partial \varphi}\left(c_p T^{*}-h^{*}\right) \quad (2)$$

where T^* and h^* are the values of T and h gained from the previous iteration and used to solve for T in current iteration. When convergence is achieved, T^* and h^* are equal to T and h, respectively, and Eq. 2 reverts to Eq. 1 since the c_pT terms on both sides cancel each other. A predefined structured mesh was used to discretize the governing equation. A more detailed description of the thermal model including the boundary conditions, numerical scheme and additional details such as air jet correlations, convection correlations, etc. can be found in Tian and Shin (2006). The model has been previously validated for a number of materials, such as hardened steels (Ding and Shin, 2010) and compact graphite iron (Skvarenina and Shin, 2006). In this study, the 3D thermal model has been extended to include a laser pre-scan process without material removal, which solved the temperature inside the workpiece before LAM. Material removal during LAM was simulated by completely or partially deactivating control volumes according to the machined workpiece geometry. As a result, the temperature inside the workpiece could be simulated continuously for both the laser pre-scan and LAM cycles. The finite volume code produces temperatures throughout the 3D workpiece, where smaller grid sizes are used within the laser spot and material removal zone for better accuracy while maintaining an acceptable computational time. Temperatures of interest in laser processing are the maximum temperature under the laser spot, average temperature in the cutting zone, and surface temperatures at locations where they can be measured during experimental trials.

The thermal model without material removal was first run to study the temperature distribution within the workpiece during the laser pre-scan process. The same values of laser power, spindle speed

and feed rate were used for laser pre-scan as well as LAM. For a 4 mm diameter laser beam with power ranging from 800 to 1200 W, the simulation results showed a uniform temperature distribution to a depth of 5 mm from the surface at the start of the workpiece after the laser scan. This provides a uniform initial temperature for LAM. Since no material removal is involved during laser pre-scan, T_{scan} is defined as the average temperature of the workpiece material within the depth of cut after the laser pre-scan step. A three-second stationary preheat-time was used at the beginning of both the laser pre-scan and LAM processes. The laser pre-scan distance was 30 mm, and it took 1.5 seconds for the laser to return to the starting position. ΔT indicates the temperature increase during LAM from T_{scan} to T_{mr}. Fig. 3 (a) and (b) show the 3D temperature distributions simulated during laser pre-scan and LAM, respectively, at a laser power (P_{CO2}) of 1000 W, cutting speed of (V) 90 m/min, feed (f) of 0.1 mm/rev, and a workpiece diameter (D) of 40 mm. T_{max} is the maximum temperature achieved as the material passes though the laser beam as shown in Fig. 3 (b), while $T_{max\text{-}tool}$ indicates the maximum temperature of the material at the tool position. To further elucidate how the laser pre-scan process increases the initial temperature in the cutting zone, the temperature histories are exemplified at two material points P1 on and P2 at a depth of cut below the surface as illustrated in Fig. 3 (c). It can be seen that the temperatures at both P1 and P2 gradually drop to T_{scan} after the laser pre-scan cycle, increase rapidly again in the LAM cycle to the maximum values as passing the laser beam, then decrease to temperatures around the average material removal temperature T_{mr} at the tool position after a time period of t_{lead} needed to travel the circumferential laser-tool lead distance.

Temperature measurement

The accuracy of the thermal model prediction mostly depends upon the accuracy of the thermophysical properties of the materials. The temperature-dependent thermal properties, as shown in

Fig. 1, were used in the thermal model. The absorptivity of a workpiece surface at a particular laser wavelength is important as this parameter represents how much laser energy is absorbed. At the CO2 laser wavelength of 10.6 μm, the absorptivity to the laser energy is 80% for a graphite coated surface (Anderson et al., 2006). To measure temperature accurately, a non-contact temperature measurement device, such as an infrared (IR) camera, requires that the emissive properties of the sample to be known. Emissivity tests were performed using a FLIR SC3000 infrared camera and three K-type thermocouples. The working bandwidth of the FLIR SC3000 infrared camera is 8-9 μm, specifications of which are given in (Anderson et al., 2006). The test samples were sectioned from the cylindrical workpiece of 56 mm in diameter and then ground to a uniform thickness of 3.6 mm. Then the sample surface was polished with a sandpaper to get the surface roughness R_a of 1 μm to mimic the machined surface. A torch was used to heat up the sample during the test and the IR camera and thermocouples recorded the top surface temperature simultaneously. Thermocouple measurements were then used to calibrate the surface emissivity by the Plank's law (Anderson et al., 2006). The emissivity test results show that the average emissivity ranges from 0.25 to 0.3 at the wavelength from 8 to 9 μm from room temperature to 500 °C.

Surface temperature measurements were conducted during LAM tests using the IR camera to validate the expanded thermal model including both laser pre-scan and LAM. The IR camera temperature measurement is schematically shown in Fig. 4 (a). The IR camera was set horizontally and 225° downstream from the tool position with a focus distance of 0.8 m. The temperature was recorded 10 frames per second during the experiment. After recording, the IR camera software was used to measure the temperature histories at multiple locations within the recorded window. For thermal model validation, the temperature histories of the center line maximum temperature and at three fixed points (P1, P2, and P3) along the central line were recorded. Emissivity of 0.85 and 0.28 was used for the

graphite coated surface and machined metal surface, respectively. A good agreement is observed between the IR camera temperature measurements and the thermal model predictions, as shown in Fig. 4 (b), which validates the accuracy of the expanded thermal model. After the laser pre-scan, the laser beam returned in the rapid mode to the starting position in 1.5 seconds without turning off the power, which caused a sudden increase in the temperatures of those three fixed points before LAM preheating. Some departing chips may have crossed the IR camera's view and caused singular points above the normal trends seen in Fig. 4 (b).

Experimental design

The thermal model was used extensively to design the LAM experiments. Faster feed rates result in less laser energy absorption and a lower temperature increase, but shorten the cooling time before LAM starts. The thermal model was used to analyze the effect of feed rate on temperature increase, and the simulation results show that T_{scan} decreases as feed increases from 0.075 to 0.3 mm/rev. The laser-tool lead distance is defined by the distance from the center of the laser beam to the edge of the machined chamfer, as shown in Fig. 2 (b), which needs to be optimized to achieve the highest T_{mr}. Preliminary simulation results show that the highest T_{mr} is obtained at a lead distance of 0.8 mm for various feed rates, and hence was chosen in all the experiments. For all the LAM experiments, a 4 mm diameter laser beam was positioned at 0.8 mm longitudinally and 55° circumferentially ahead of the tool position.

It is desirable that a parametric relationship be developed to determine the average material removal temperature due to laser heating as a function of machining, laser, and workpiece parameters. A multivariable regression analysis using simulation data was conducted to establish a parametric model, which determines the average material removal temperature during the LAM process. Four

independent variables, CO_2 laser power, workpiece diameter, cutting speed, and feed were selected as the four factors for this statistical analysis. The obtained equations predict the average material removal temperature with an estimation error less than 10°C. For T_{scan} achieved after the laser pre-scan process, the following regression models were derived for 27%Cr and 35%Cr based on the simulation results:

$$T_{scan,27\%Cr} = 40.5\frac{P_{CO2}^{0.77}}{D^{0.88}V^{0.33}f^{0.33}} \quad (3)$$

$$T_{scan,35\%Cr} = 21.1\frac{P_{CO2}^{0.81}}{D^{0.46}V^{0.37}f^{0.34}} \quad (4)$$

For T_{mr} during LAM, the following regression models were derived:

$$T_{mr,27\%Cr} = 13.3\frac{P_{CO2}^{0.56}f^{0.005}}{D^{0.5}V^{0.03}}T_{scan,27\%Cr}^{0.31} \quad (5)$$

$$T_{mr,35\%Cr} = 24.0\frac{P_{CO2}^{0.57}f^{0.01}}{D^{0.67}V^{0.003}}T_{scan,35\%Cr}^{0.27} \quad (6)$$

Eqs. 3-6 have been used extensively to determine the laser parameters in the LAM experiments.

EXPERIMENTAL RESULTS

LAM experiments were conducted for 27%Cr and 35%Cr. The machinability and surface integrity of these materials are discussed in great detail as follows.

Cutting force

To study the temperature effect, LAM tests were conducted for both 27%Cr and 35%Cr with a cutting speed of 90 m/min, feed of 0.1 mm/rev, depth of cut of 0.76 mm, and varying T_{mr} from room temperature to 500 °C. These tests are aimed to determine the critical T_{mr}, beyond which the cutting force will be reduced greatly while the surface integrity remains the same or becomes better. Fig. 5 (a)

compares the cutting forces in conventional cutting and LAM of 27%Cr with T_{mr} ranging from 300 to 500 °C. It can be seen that increasing T_{mr} greatly reduces the cutting forces in all three directions. The tangential cutting force (F_c) was reduced by 21%, 28% and 31% as the T_{mr} increased from room temperature to 300, 400 and 500 °C, respectively. Similar amounts of force reductions were also found in the feed (F_f) and radial (F_t) directions. For 35%Cr, the thrust and feed forces increased more rapidly and became larger than the tangential cutting force after a short period of cutting without laser-assist, which indicated that the insert had worn out quickly. In fact, the insert fractured immediately in a following test during conventional cutting. In contrast, the force components in all three directions increased very slowly during the LAM tests of 35%Cr.

Since the magnitude of the cutting force largely depended on the actual depth of cut, the specific cutting energy was calculated for all the tests, as can been in Fig. 5 (b). Compared to conventional machining, the specific cutting energy of 27%Cr and 35%Cr during LAM decreased by approximately 28% and 26%, respectively, as T_{mr} increased to 400°C. The specific cutting energy of 35%Cr was about 25% higher than that of 27%Cr at the same temperature due to its higher mechanical strength. Increasing the temperature to 500 °C led to a further reduction of the cutting force for both materials. However, the color of the machined surface turned to a light brownish hue due to oxidation in the air, as can be seen in Fig. 6. T_{mr} less than 450 °C does not induce any discoloration; therefore, T_{mr} of 400 °C was chosen to be the optimum temperature to avoid oxidization of the machined surface after LAM of both 27%Cr and 35%Cr.

The cutting force during LAM of 27%Cr increased slightly as the tool wore, as can be seen in Fig. 5 (c). For a speed of 90 m/min, the tangential cutting force increased by about 17% after 12.9 min of cutting time. The magnitudes of the feed and thrust force were less than that of the tangential force, even when the tool was significantly worn. Fig. 5 (d) shows the progression of the cutting forces in

LAM of 35%Cr. For a fresh cutting edge, the tangential cutting force was the largest one of all three force components. As the tool wore, the thrust force and feed force increased more rapidly than the tangential cutting force and became 30-50% larger than the tangential force when the tool was significantly worn. The thrust and feed force developed at a similar rate as the tool wore down. The decrease in cutting force in LAM enabled a longer tool life than that in conventional cutting.

Tool wear progression

T_{mr} of 400 °C was selected as the optimum temperature in LAM of both 27%Cr and 35%Cr. Crater wear and flank wear were found to be the main tool wear modes. When the crater wear approaches the cutting edge, edge chipping or fracture will occur. When the crater wear depth reaches a critical value, the tool will also fail. The widths of the flank and crater wear were measured to quantitatively study the tool wear rates. Fig. 7 (a) and (b) compare the tool crater and flank wear progression of the CBN inserts at various cutting speeds between conventional cutting and LAM of 27%Cr. For machining 27%Cr with a cutting speed less than 90 m/min, crater wear was the primary tool wear mode for both conventional and LAM conditions, while tool flank wear developed at a slower rate. As the cutting speed exceeded 90 m/min, tool flank wear became the primary mode and developed more quickly. Increasing T_{mr} to 400 °C was found to be very beneficial to reduce the amount of tool wear. Fig. 7 (a) shows that the crater wear progression rate at a cutting speed of 90 m/min was reduced by half as T_{mr} is increased from room temperature to 400 °C, while Fig. 7 (b) shows that the flank wear progression rate at a cutting speed of 150 m/min was reduced by half as well.

Due to the higher strength and hardness of 35%Cr, the CBN insert fractured after 1 minute during conventional cutting at a cutting speed of 90 m/min on the CNC lathe. The tool fractured immediately when it entered the workpiece at a higher speed of 150 m/min. The machinability of

35%Cr was so poor that no more conventional cutting tests were conducted with the CBN inserts. Much longer tool life was achieved under a LAM condition with the same CBN inserts. Fig. 8 compares the tool wear progressions of the CBN inserts at various cutting speeds for LAM of 35%Cr using a T_{mr} of 400 °C. For 35%Cr, flank wear was the primary mode for various cutting speeds tested. As the cutting speed increased from 90 to 150 m/min, the tool life decreased significantly from 12.4 to 1.1 minutes under LAM conditions. LAM tool life tests of 35%Cr were repeated at speeds of 120 and 150 m/min with the CBN inserts and show good repeatability as can be seen in Fig. 8. Images of flank wear are shown in Fig. 8 for LAM of 35%Cr at various cutting speeds. It can be seen that the tool flank wear was the dominant tool wear mode for both 90 and 150 m/min.

Chips were collected to study the trend of the chip formation after the cutting tests. Chip morphology is an important attribute of the cutting process. For conventional cutting, initially the generated chip was very short and was golden in color. As the tool wore, the chip became longer and the color became purple or cyan. For LAM, the chip generated initially was short (but longer than those produced by conventional cutting) and the color was bluish. As the tool wore, the chip color became cyan. As a result, chip color and length can be used as an indicator for overall tool wear.

Surface integrity

LAM produced parts with a consistent, smooth surface finish. Surface roughness R_a did not deteriorate as tool wear developed. Fig. 9 shows the progression of the surface finish of the 27%Cr and 35%Cr parts produced by LAM and conventional cutting. The surface finish for 27%Cr is consistently better than 35%Cr, although surface roughness produced by conventional cutting was generally more than 1 µm as can be seen in Fig. 9 a and b. The surface finish of 35%Cr by conventional cutting was poor, resulting in a roughness R_a as high as 3 µm. The surface roughness was much improved to

consistently around 1µm for LAM even when the tool was worn as can be seen in Fig. 9 c and d. The variation of the surface roughness produced by conventional cutting was about 1 µm, which is much more than that of the surface produced by LAM. Many small metal powders were deposited on the machined surface after conventional cutting. Fig. 10 a and b show the microscopic images of surfaces of 27%Cr samples machined at 150 m/min, while c and d shows the three dimensional surface profiles taken by a non-contact interferometric surface profiler. High peaks with a maximum magnitude of 6 µm can be seen on the machined surface produced by conventional cutting, while uniform peaks of 2 µm maximum magnitude can be seen on the LAM surface.

Multiple specimens were used to study the microstructure and to measure the subsurface microhardness for LAM and conventional cutting of 27%Cr and 35%Cr. Fig. 11 a-d show the subsurface microstructures after conventional cutting and LAM of 27%Cr and 35%Cr. Fig. 11 a and b were obtained approximately 30 µm below the machined surface, c was obtained 2 mm below the surface to represent the unaffected zone, d was taken at the surface. The micrographs show that a greater amount of chromium carbides exists in 35%Cr samples than in 27%Cr parts. No microstructural change was observed when comparing the machined subsurface after conventional machining with those after LAM. This is explained by the fact that the bulk temperature is increased to around 400°C during LAM and the temperature only lasts for a few minutes. Tempering in such a short period of time does not introduce a significant microstructural change during LAM.

Surface hardness was measured on the machined surface by using a Mitutoyo ATK-F1000 hardness tester with a Rockwell C tip. Subsurface microhardness was measured by using a LECO microhardness tester LM247AT with a Vickers diamond tip with a diagonal of 50 µm. The Vickers hardness tests were carried out on the specimens with a load of 1 kgf. Although smaller loads were available, more accurate measurement was achieved with a larger load of 1 kgf for the highly

inhomogeneous microstructures of the two materials (Lampman, 2000). The distance between two adjacent measurements was 100 µm. Fig. 12 shows that the subsurface microhardness is constant within 1 mm below the machined surface after LAM or conventional cutting for both materials. The surface hardness measurement was performed at multiple (greater than 3) locations for each as-received part. It was found that the surface hardness was 60±3 HRC for 27%Cr and 66±5.5 HRC for 35%Cr, respectively. The average hardness of the 27%Cr specimen produced by conventional cutting at a speed of 90 m/min was lower than the other three specimens, as can be seen in Fig. 12, which was mostly caused by the lower initial hardness of the particular sample. Fig. 12 proves that LAM does not decrease the hardness of the part surface and subsurface.

Tool life and process map

Maximum flank wear width of 0.45 mm and crater wear width of 0.3 mm were chosen as the tool wear limits used in this tool wear study. For all the test conditions, the tool wear progressed in a linear fashion before reaching the tool wear limit defined above. After reaching the limits, the worn CBN inserts would show a rapid progression to gross tool fracture. Such a catastrophic tool failure is very detrimental to machine tool equipment and workpiece. To avoid the catastrophic fracture, the tool wear experiments were stopped before the tools exceeded the limits.

Similar tool life criteria have been used in other experimental studies of hard turning using CBN tools (Bouchelaghem et al., 2010; Arsecularatne and Mathew, 2000) as well. The increase of cutting force, deterioration of the surface finish and change of the chip morphology all worked as signs of tool failure during the tool wear tests. A linear fit for tool wear data was accurate to delineate the tool wear progression before reaching the tool wear limits. As the tool wear reaches the limits, the tool was considered “failed” in this study, and the tool life value was derived based on the tool wear limits defined above. Table 2 summarizes the results of tool wear tests for 27%Cr and 35%Cr.

Experimental results of 27%Cr and 35%Cr show the effects of cutting speed, temperature and workpiece material microstructure on the CBN tool life. For instance, for 27%Cr, as the cutting speed increased from 90 to 150 m/min, the tool life decreased significantly from 18.3 to 4.56 minutes for conventional cutting and from 35.6 to 9.1 min for LAM conditions. To effectively design the LAM process for high chromium white irons with different microstructures, it is necessary to quantitatively analyze the contribution of these factors to the cutting tool life. The following empirical formula was derived for CBN tool life in cutting of high chromium white irons from the experimental results, considering the effects of cutting speed, hardness and temperature:

$$T_{life} = 4.12\left(\frac{V}{60}\right)^{-3.09}\left(\frac{H}{70}\right)^{-17.14}\left(\frac{T_{\mathrm{mr}}+273.15}{300}\right)^{1.19} \quad (7)$$

where T_{life} is the ideal tool life in minutes, V is the cutting speed in m/min, H is the initial bulk hardness in HRC of the workpiece material and T_{mr} is the average material removal temperature in Celsius degree. The cutting speed, workpiece bulk hardness and material removal temperature are normalized in Eq. 7 by a speed of 60 m/min, a hardness of 70 HRC and a temperature of 300 K, respectively. The tool life data predicted by Eq. 7 is compared with the experimental data in Fig. 13 for various conditions and different high chromium white irons. A good agreement can be seen between the predictions and the tool life data obtained through experiments. It is apparent that the tool life achieved by LAM at least doubles the value obtained under conventional cutting at a same condition. The material removal rate can also be greatly improved by using the LAM process. For example, for machining of 27%Cr with a minimum tool life of 10 minutes, the highest cutting speed of 105 m/min using a conventional cutting process can be increased to 140 m/min under a LAM condition. The machining cost for 35%Cr is very high due to a very short tool life, while LAM improves its machinability by increasing the tool life to 10-25 minutes while pushing the cutting speed to 70-90 m/min.

Compared with the other empirical tool life models for CBN cutting tools proposed in (Al-Ahmari, 2007; Sahin, 2009; Arsecularatne et al., 2006), Eq. 7 considers the initial workpiece microstructural property and average material removal temperature in the cutting zone, and hence is useful in designing an LAM process for high chromium white irons with different microstructures. For instance, for 30%Cr with a bulk hardness of 62 HRC between those of 27%Cr and 35%Cr, Eq. 7 shows that increasing T_{mr} to 400 °C prolongs the CBN tool life from 8 minutes to around 24 minutes at a cutting speed of 90 m/min. The total manufacturing cost can also be optimized using Eq. 7 to achieve the balance of maximizing the material removal rate while maintaining a good tool life. The highlighted area in Fig. 13 indicates the preferable LAM conditions using CBN tools for high chromium irons with different microstructures.

CONCLUSIONS

The machinability of 27%Cr and 35%Cr materials were experimentally analyzed during laser-assisted machining with varying heating and operating conditions. A laser pre-scan process was designed to preheat the workpiece before LAM and a 3D thermal model was used to correctly predict the temperature inside the workpiece during the two-step process of laser pre-scan and LAM. T_{mr} of 400°C was found to be the optimum temperature during LAM and it reduced the tangential cutting force by 28% and 26% for 27%Cr and 35%Cr, respectively. LAM produced the parts of a consistently smooth surface finish with R_a of 0.8 µm. Surface roughness produced by conventional cutting was more than 1 µm and many small metal powders were observed to be stuck on the machined surface. The subsurface microhardness remains relatively constant within 1 mm below the machined surface after LAM and conventional cutting for both materials. Compared with conventional machining, no microstructural change was introduced by the two-step LAM process. Extensive tool wear tests

conducted under both LAM and conventional cutting conditions revealed LAM doubled the tool life for the cutting of 27%Cr at various cutting speeds. For the harder material 35%Cr, LAM improved the tool life by a factor of 10. An empirical tool life formula derived from the tool wear experiments was shown to be a useful tool to design the LAM process using CBN tools and improve the machinability of high chromium white irons.

NOMENCLATURE

a_p	depth of cut
D	workpiece diameter
f	feed
F_c	tangential cutting force component
F_f	cutting force component in the feed direction
F_t	cutting force component in the radial direction
h	enthalpy
h^*	enthalpy gained from the previous iteration
H	initial bulk hardness
P_{CO2}	CO_2 laser power
r_n	cutting tool nose radius
T	temperature
T^*	temperature gained from the previous iteration
t_{lead}	time needed to travel the circumferential laser-tool lead distance
T_{life}	tool life

T_{max}	maximum temperature
$T_{max\text{-}tool}$	maximum temperature at the tool position
T_{mr}	average material removal temperature
T_{scan}	average temperature within the depth of cut after the laser pre-scan step
V	cutting speed
ΔT	temperature increase during LAM from T_{scan} to T_{mr}
ρ	density
ω	angular velocity

REFERENCES

Al-Ahmari, A.M.A. (2007) Predictive machinability models for a selected hard material in turning operations. Journal of Materials Processing Technology, 190: 305-311.

Anderson, M.; Patwa, R.; Shin, Y.C. (2006) Laser-assisted machining of Inconel 718 with an economic analysis. International Journal of Machine Tools and Manufacture, 46: 1879-1891.

Arsecularatne, J.A.; Mathew, P. (2000) Prediction of tool life in machining with restricted contact tools. Machining Science and Technology, 4: 177-196.

Arsecularatne, J.A.; Zhang, L.C.; Montross, C. (2006) Wear and tool life of tungsten carbide, PCBN and PCD cutting tools. International Journal of Machine Tools and Manufacture, 46: 482-491.

Belyakova, P.E.; Garber, M.E.; Rozhkova, E.V. (1975) Physical properties of white chromium cast irons. Metal Science and Heat Treatment, 17: 1041-1044.

Bouchelaghem, H.; Yallese, M.A.; Mabrouki, T.; Amirat, A.; Rigal, J.F. (2010) Experimental investigation and performance analyses of CBN insert in hard turning of cold work tool steel (D3). Machining Science and Technology, 14: 471-501.

Dandekar, C.R.; Shin, Y.C.; Barnes, J. (2010) Machinability improvement of titanium alloy (Ti-6Al-4V) via LAM and hybrid machining. International Journal of Machine Tools and Manufacture, 50: 174-182.

Davis, J.R. (1996) Cast Irons (ASM Specialty Handbook). ASM international, Materials Park, OH,

Ding, H.; Shin, Y.C. (2010) Laser-assisted machining of hardened steel parts with surface integrity analysis. International Journal of Machine Tools and Manufacture, 50: 106-114.

Ding, H.; Shin, Y.C. (2012) Improvement of machinability of waspaloy via laser-assisted machining. International Journal of Advanced Manufacturing Technology, In Press, DOI: 101007/s00170-012-4012-8:

Germain, G.; Dal Santo, P.; Lebrun, J.L. (2011) Comprehension of chip formation in laser assisted machining. International Journal of Machine Tools and Manufacture, 51: 230-238.

Lampman, S.R. (ed) (2000) Mechanical Testing and Evaluation, vol 8. ASM Handbook, 8 edn. ASM International, Materials Park, OH,

Lampman, S.R.; Zorc, T.B. (eds) (1990) Properties and Selection: Irons, Steels, and High-performance Alloys, vol 1. Metals Handbook, 10 edn. ASM International, Materials Park, OH,

Masood, S.H.; Armitage, K.; Brandt, M. (2011) An experimental study of laser-assisted machining of hard-to-wear white cast iron. International Journal of Machine Tools and Manufacture, 51: 450-456.

Ren, X.J.; James, R.D.; Brookes, E.J.; Wang, L. (2001) Machining of high chromium hardfacing materials. Journal of Materials Processing Technology, 115: 423-429.

Rozzi, J.C.; Pfefferkorn, F.E.; Incropera, F.P.; Shin, Y.C. (2000) Transient, three-dimensional heat transfer model for the laser assisted machining of silicon nitride: I. Comparison of predictions

with measured surface temperature histories. International Journal of Heat and Mass Transfer, 43: 1409-1424.

Sahin, Y. (2009) Comparison of tool life between ceramic and cubic boron nitride (CBN) cutting tools when machining hardened steels. Journal of Materials Processing Technology, 209: 3478-3489.

Shen, H.C.; Zong, W.S.; Nie, J.J.; Wang, J. Study on high-speed cutting of Hi-Cr cast iron impeller and sheath of slurry pump using overall PCBN cutting tools. In: 2010 International Conference on Computer, Mechatronics, Control and Electronic Engineering, CMCE 2010, August 24, 2010 - August 26, 2010, Changchun, China, 2010. IEEE Computer Society, pp 535-538

Skvarenina, S.; Shin, Y.C. (2006) Laser-assisted machining of compacted graphite iron. International Journal of Machine Tools and Manufacture, 46: 7-17.

Sun, S.; Brandt, M.; Dargusch, M.S. (2010) Thermally enhanced machining of hard-to-machine materials—A review. International Journal of Machine Tools and Manufacture, 50: 663-680.

Suthar, K.J.; Patten, J.; Dong, L.; Abdel-Aal, H. Estimation of temperature distribution in silicon during micro laser assisted machining. In: International Manufacturing Science and Engineering Conference, Evanston, Illinois, USA, October 7-10 2008. Proceedings of the 2008 International Manufacturing Science and Engineering Conference, MSEC2008-72195.

Tabrett, C.P.; Sare, I.R.; Ghomashchi, M.R. (1996) Microstructure-property relationships in high chromium white iron alloys. International Materials Reviews, 41: 59-82.

Tian, Y.; Shin, Y.C. (2006) Thermal modeling for laser-assisted machining of silicon nitride ceramics with complex features. Journal of Manufacturing Science and Engineering, Transactions of the ASME, 128: 425-434.

Zhou, J.M.; Andersson, M. (2008) Machinability of Abrasion Resistance Cast Iron with PCBN Cutting Tools. Materials and Manufacturing Processes, 23: 506-512.

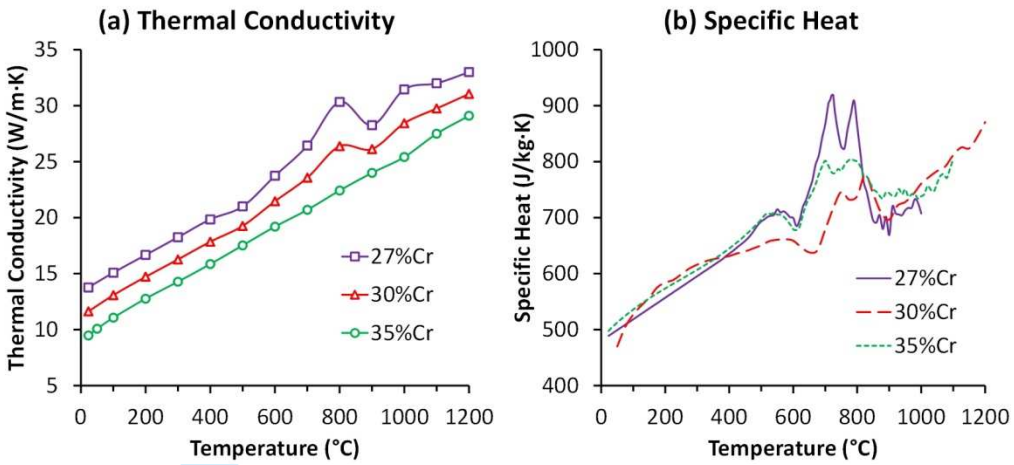

Fig. 1 Thermal properties at elevated temperatures

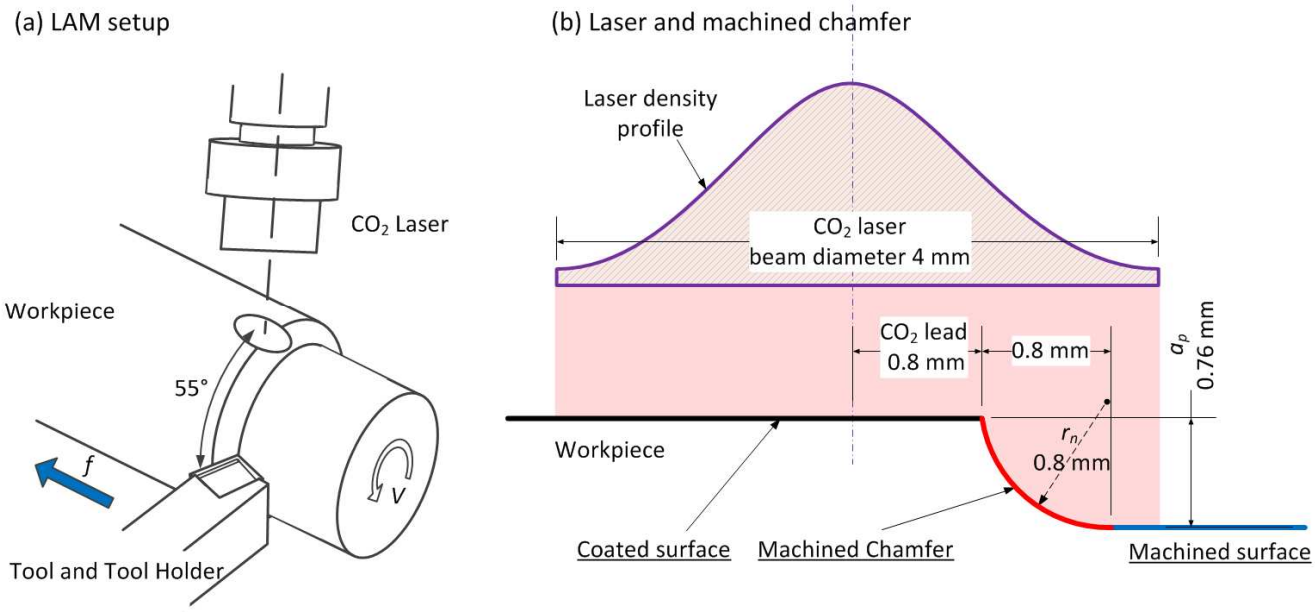

Fig. 2 Experimental setup

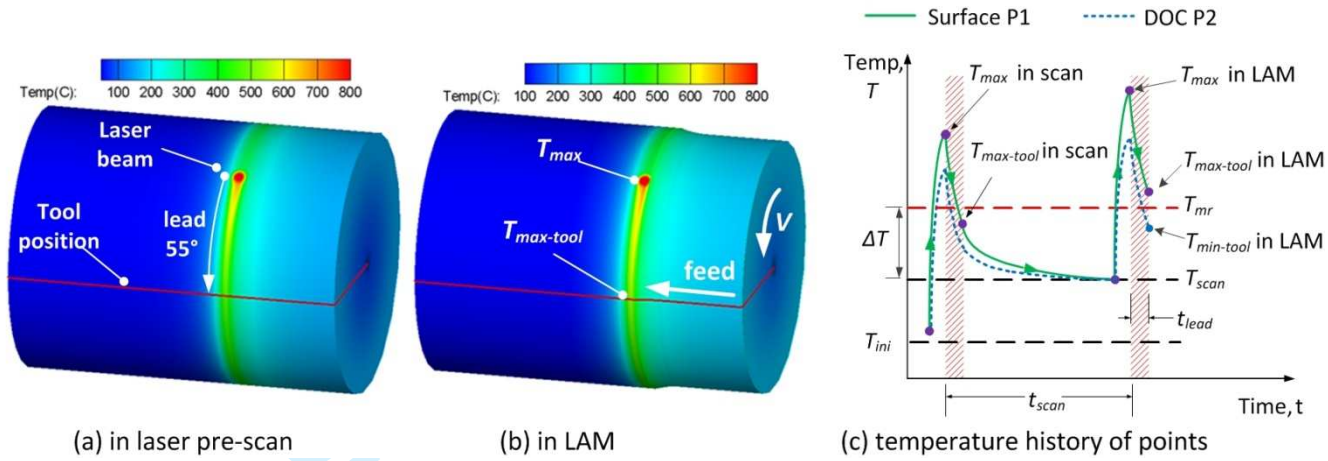

(a) in laser pre-scan (b) in LAM (c) temperature history of points

Fig. 3 Temperature predictions of LAM of 27%Cr with laser pre-scan under the condition: P_{CO2}=1000 W, V=90 m/min, f=0.1 mm/rev and D=40 mm.

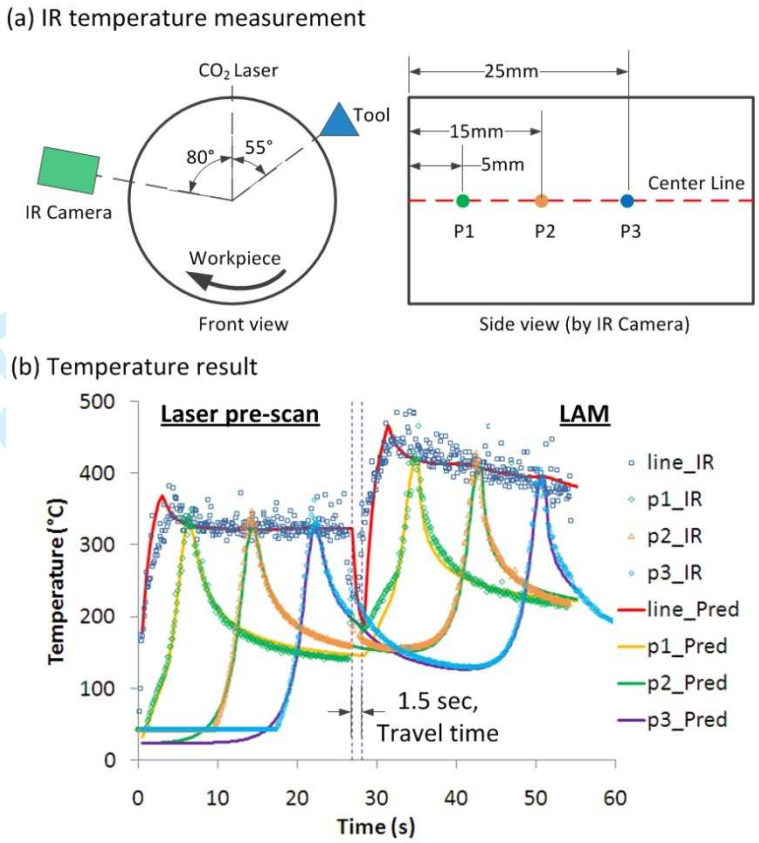

Fig. 4 Comparisons of the IR camera measurements and the thermal model predictions during LAM of 27%Cr. Experimental conditions: P_{CO2}=884 W, V=90 m/min, f=0.1 mm/rev and D=35.3 mm.

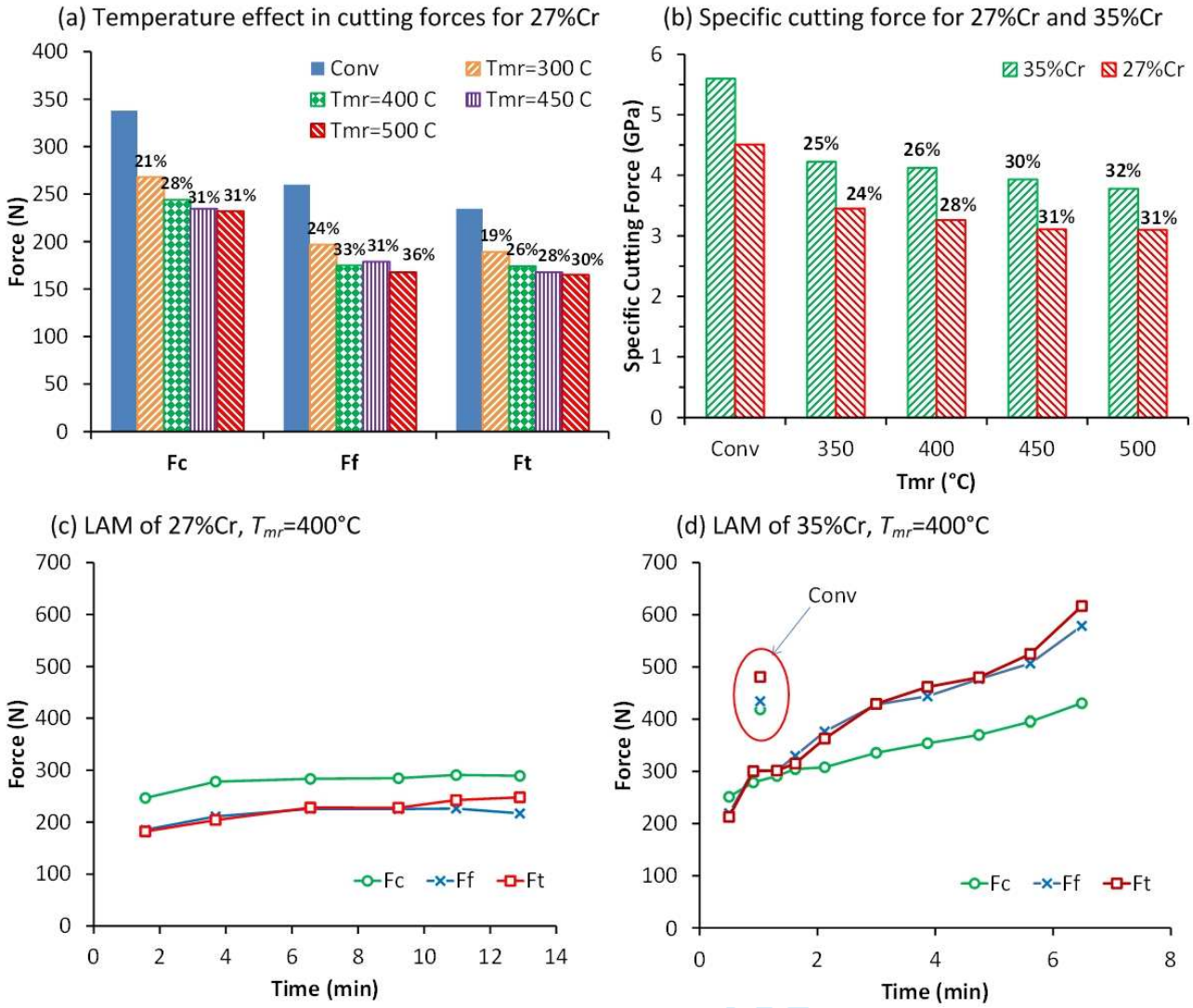

Fig. 5 Temperature effect on cutting force during LAM of 27%Cr and 35%Cr

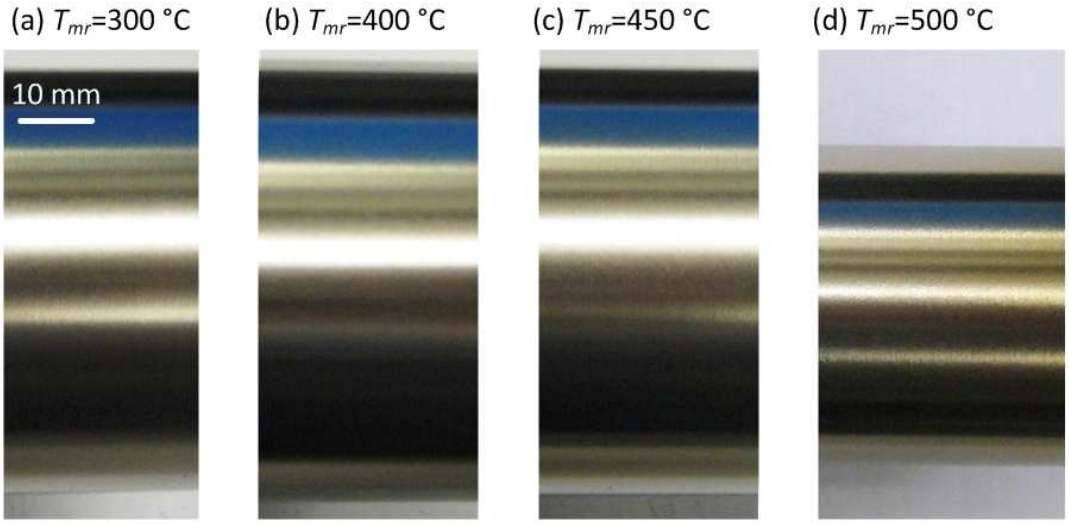

Fig. 6 Machined surface after LAM of 27%Cr

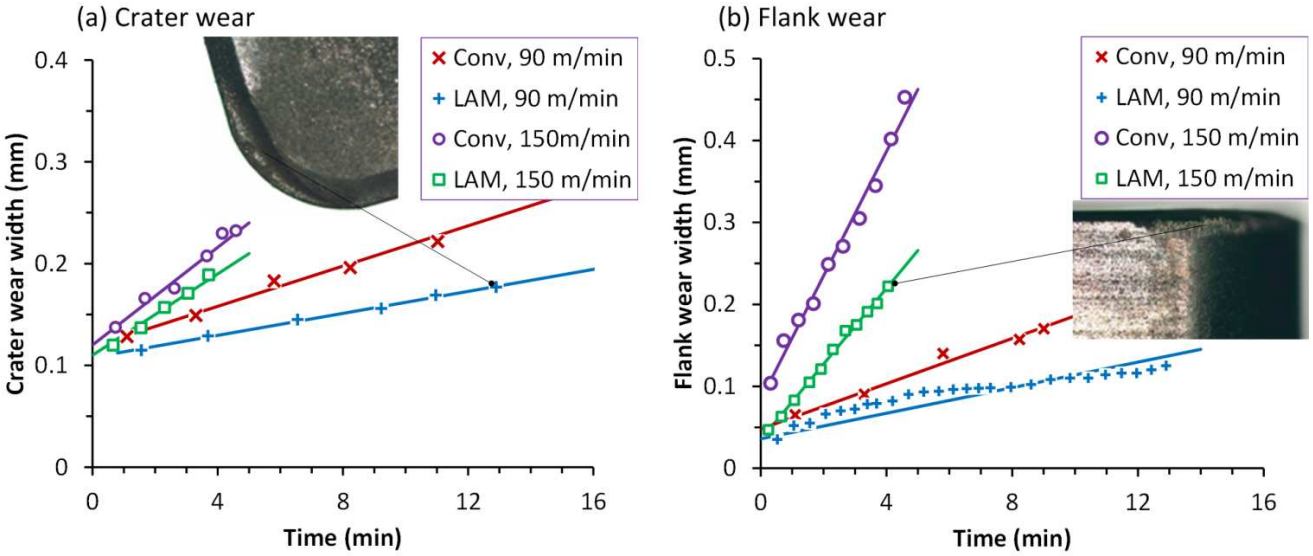

Fig. 7 Tool wear progressions for 27%Cr: (a) Crater wear, (b) Flank wear

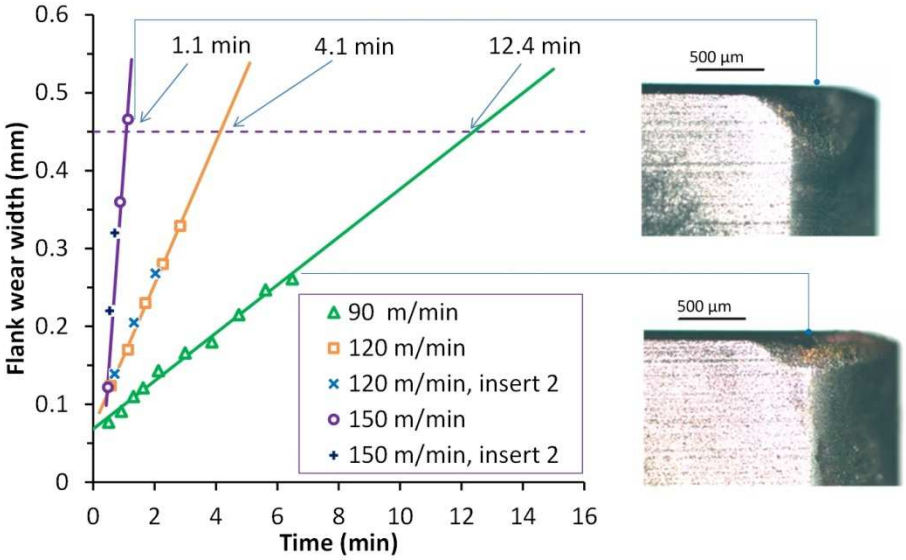

Fig. 8 Tool wear progression in LAM of 35%Cr.

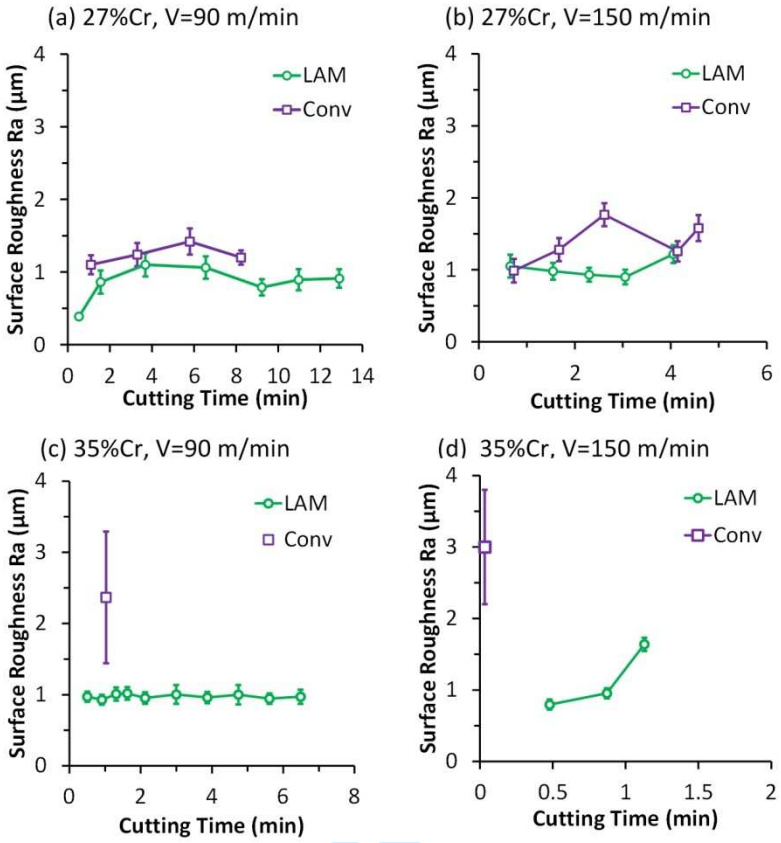

Fig. 9 Surface finish progressions

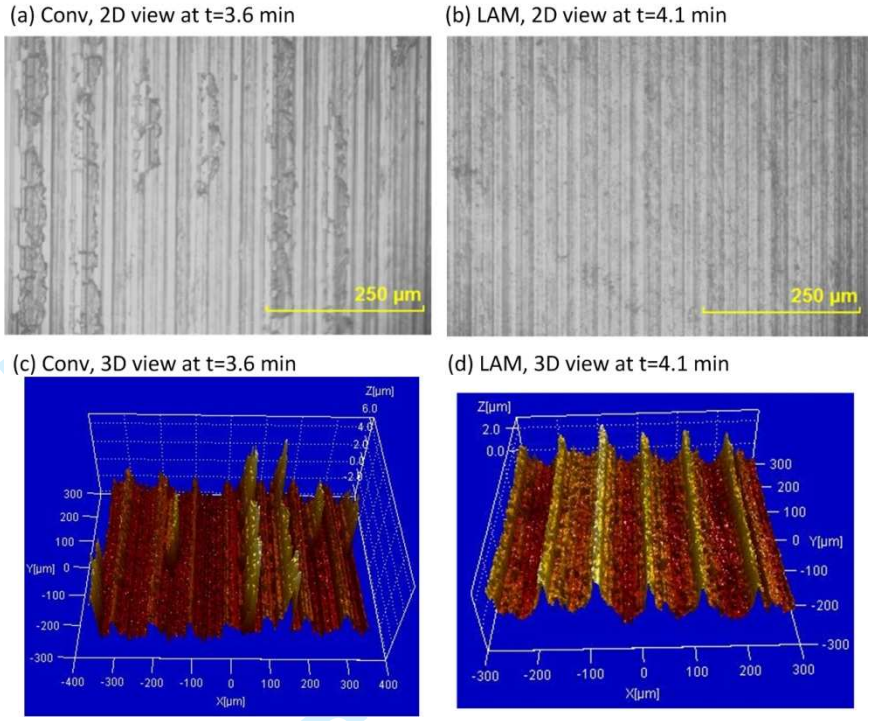

Fig. 10 Surface profiles of 27%Cr samples machined at 150 m/min

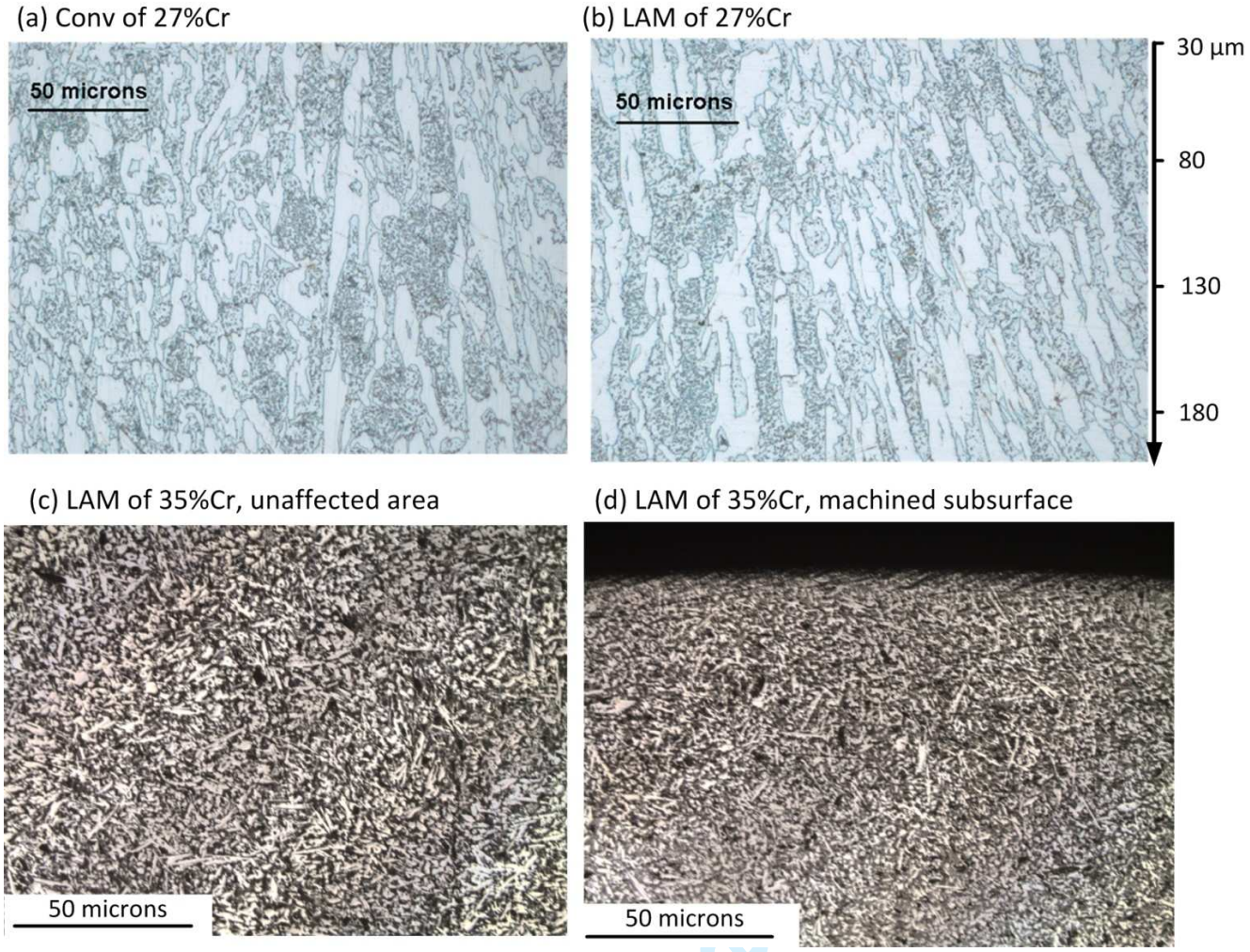

Fig. 11 Optical microscopy (500X) of microstructures of the machined subsurface produced by LAM and conventional cutting at a speed of 90 m/min.

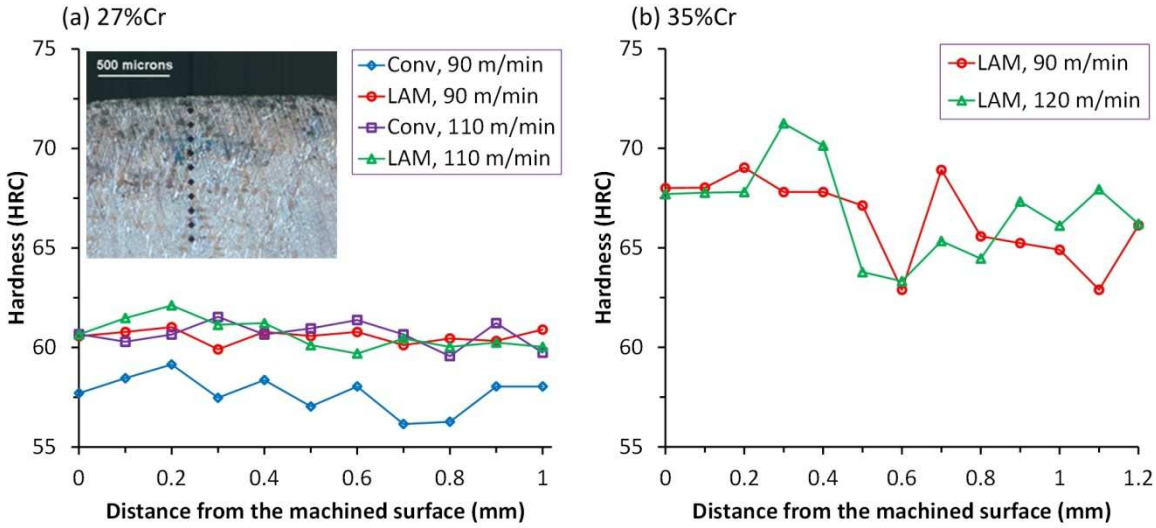

Fig. 12 Subsurface microhardness of parts produced by LAM and conventional cutting

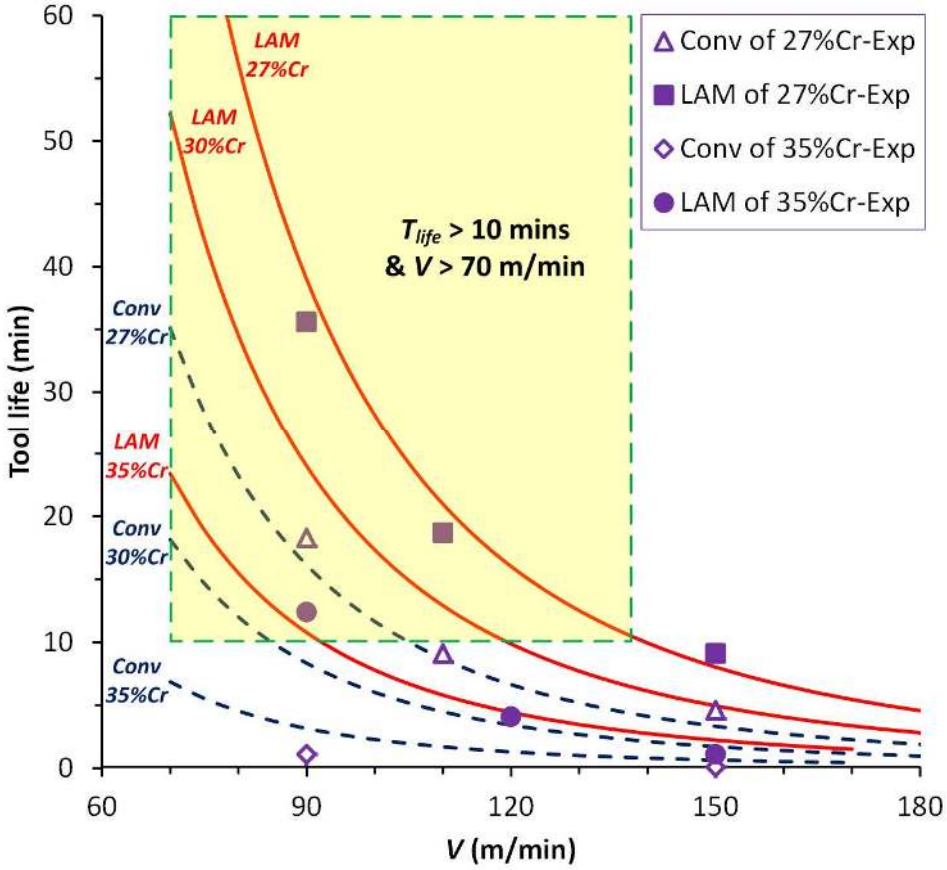

Fig. 13 CBN tool life map for high chromium white irons.

Table 1 Phase compositions and volume fractions

Alloys	Primary carbides (M_3C)	Eutectic carbides (M_7C_3)	Total carbides	Matrix	Hardness H (HRC)	Density ρ (kg/m^3)
27%Cr	≈0	28%	28%	72%	60±3	7,500
30%Cr	26%	21%	47%	53%	≈62	7,470
35%Cr	39%	19%	58%	42%	66±5.5	7,500

Table 2 Tool wear tests for 27%Cr and 35%Cr

Material	Condition	V (m/min)	f (mm/rev)	a_p (mm)	T_{mr} (°C)	Tool life (min)
27%Cr	27%Cr-Conv1	90	0.1	0.76	24	18.3
	27%Cr-Conv2	110	0.1	0.76	24	9.0
	27%Cr-Conv3	150	0.1	0.76	24	4.6
	27%Cr-LAM1	90	0.1	0.76	400	35.6
	27%Cr-LAM2	110	0.1	0.76	400	18.7
	27%Cr-LAM3	150	0.1	0.76	400	9.1
35%Cr	35%Cr-Conv1	90	0.1	0.76	24	1
	35%Cr-Conv3	150	0.1	0.76	24	0.1
	35%Cr-LAM1	90	0.1	0.76	400	12.4
	35%Cr-LAM2	120	0.1	0.76	400	4.1
	35%Cr-LAM3	150	0.1	0.76	400	1.1

Al-Ahmari, A.M.A. (2007) Predictive machinability models for a selected hard material in turning operations. Journal of Materials Processing Technology, 190: 305-311.

Anderson, M.; Patwa, R.; Shin, Y.C. (2006) Laser-assisted machining of Inconel 718 with an economic analysis. International Journal of Machine Tools and Manufacture, 46: 1879-1891.

Arsecularatne, J.A.; Mathew, P. (2000) Prediction of tool life in machining with restricted contact tools. Machining Science and Technology, 4: 177-196.

Arsecularatne, J.A.; Zhang, L.C.; Montross, C. (2006) Wear and tool life of tungsten carbide, PCBN and PCD cutting tools. International Journal of Machine Tools and Manufacture, 46: 482-491.

Belyakova, P.E.; Garber, M.E.; Rozhkova, E.V. (1975) Physical properties of white chromium cast irons. Metal Science and Heat Treatment, 17: 1041-1044.

Bouchelaghem, H.; Yallese, M.A.; Mabrouki, T.; Amirat, A.; Rigal, J.F. (2010) Experimental investigation and performance analyses of CBN insert in hard turning of cold work tool steel (D3). Machining Science and Technology, 14: 471-501.

Dandekar, C.R.; Shin, Y.C.; Barnes, J. (2010) Machinability improvement of titanium alloy (Ti-6Al-4V) via LAM and hybrid machining. International Journal of Machine Tools and Manufacture, 50: 174-182.

Davis, J.R. (1996) Cast Irons (ASM Specialty Handbook). ASM international, Materials Park, OH,

Ding, H.; Shin, Y.C. (2010) Laser-assisted machining of hardened steel parts with surface integrity analysis. International Journal of Machine Tools and Manufacture, 50: 106-114.

Ding, H.; Shin, Y.C. (2012) Improvement of machinability of waspaloy via laser-assisted machining. International Journal of Advanced Manufacturing Technology, In Press, DOI: 101007/s00170-012-4012-8:

Germain, G.; Dal Santo, P.; Lebrun, J.L. (2011) Comprehension of chip formation in laser assisted machining. International Journal of Machine Tools and Manufacture, 51: 230-238.

Lampman, S.R. (ed) (2000) Mechanical Testing and Evaluation, vol 8. ASM Handbook, 8 edn. ASM International, Materials Park, OH,

Lampman, S.R.; Zorc, T.B. (eds) (1990) Properties and Selection: Irons, Steels, and High-performance Alloys, vol 1. Metals Handbook, 10 edn. ASM International, Materials Park, OH,

Masood, S.H.; Armitage, K.; Brandt, M. (2011) An experimental study of laser-assisted machining of hard-to-wear white cast iron. International Journal of Machine Tools and Manufacture, 51: 450-456.

Ren, X.J.; James, R.D.; Brookes, E.J.; Wang, L. (2001) Machining of high chromium hardfacing materials. Journal of Materials Processing Technology, 115: 423-429.

Rozzi, J.C.; Pfefferkorn, F.E.; Incropera, F.P.; Shin, Y.C. (2000) Transient, three-dimensional heat transfer model for the laser assisted machining of silicon nitride: I. Comparison of predictions with measured surface temperature histories. International Journal of Heat and Mass Transfer, 43: 1409-1424.

Sahin, Y. (2009) Comparison of tool life between ceramic and cubic boron nitride (CBN) cutting tools when machining hardened steels. Journal of Materials Processing Technology, 209: 3478-3489.

Shen, H.C.; Zong, W.S.; Nie, J.J.; Wang, J. Study on high-speed cutting of Hi-Cr cast iron impeller and sheath of slurry pump using overall PCBN cutting tools. In: 2010 International Conference on Computer, Mechatronics, Control and Electronic Engineering, CMCE 2010, August 24, 2010 - August 26, 2010, Changchun, China, 2010. IEEE Computer Society, pp 535-538

Skvarenina, S.; Shin, Y.C. (2006) Laser-assisted machining of compacted graphite iron. International Journal of Machine Tools and Manufacture, 46: 7-17.

Sun, S.; Brandt, M.; Dargusch, M.S. (2010) Thermally enhanced machining of hard-to-machine materials—A review. International Journal of Machine Tools and Manufacture, 50: 663-680.

Suthar, K.J.; Patten, J.; Dong, L.; Abdel-Aal, H. Estimation of Temperature Distribution in Silicon During Micro Laser Assisted Machining. In: International Manufacturing Science and Engineering Conference, Evanston, Illinois, USA, October 7-10 2008. Proceedings of the 2008 International Manufacturing Science and Engineering Conference, MSEC2008-72195.

Tabrett, C.P.; Sare, I.R.; Ghomashchi, M.R. (1996) Microstructure-property relationships in high chromium white iron alloys. International Materials Reviews, 41: 59-82.

Tian, Y.; Shin, Y.C. (2006) Thermal modeling for laser-assisted machining of silicon nitride ceramics with complex features. Journal of Manufacturing Science and Engineering, Transactions of the ASME, 128: 425-434.

Zhou, J.M.; Andersson, M. (2008) Machinability of Abrasion Resistance Cast Iron with PCBN Cutting Tools. Materials and Manufacturing Processes, 23: 506-512.